European Journal of Medicinal Chemistry 222 (2021) 113562

Contents lists available at ScienceDirect

European Journal of Medicinal Chemistry

journal homepage: http://www.elsevier.com/locate/ejmech

Optimization of the clofazimine structure leads to a highly water-soluble C3-aminopyridinyl riminophenazine endowed with improved anti-Wnt and anti-cancer activity *in vitro* and *in vivo*

Alexey Koval [a, 1], Ivan Bassanini [b, k, 1], Jiabin Xu [a, c, 1], Michele Tonelli [d], Vito Boido [d], Fabio Sparatore [d], Frederic Amant [e, f, g], Daniela Annibali [e], Eleonora Leucci [h, i], Anna Sparatore [b, 2, **], Vladimir L. Katanaev [a, j, 2, *]

[a] *Department of Cell Physiology and Metabolism, Translational Research Centre in Oncohaematology, Faculty of Medicine, University of Geneva, 1206, Geneva, Switzerland*
[b] *Dipartimento di Scienze Farmaceutiche, Università degli Studi di Milano, 20133, Milano, Italy*
[c] *Department of Biomedical Sciences, Faculty of Biology and Medicine, 1011, University of Lausanne, Lausanne, Switzerland*
[d] *Dipartimento di Farmacia, Università di Genova, 16132, Genova, Italy*
[e] *Gynecological Oncology Laboratory, Department of Oncology, KU Leuven and Leuven Cancer Institute (LKI), 3000, Leuven, Belgium*
[f] *Department of Obstetrics and Gynecology, University Hospitals Leuven and Department of Oncology, 3000, Leuven, Belgium*
[g] *Centre for Gynecologic Oncology Amsterdam (CGOA), Antoni Van Leeuwenhoek-Netherlands Cancer Institute (AvL-NKI), University Medical Center (UMC), 1066, Amsterdam, the Netherlands*
[h] *Laboratory for RNA Cancer Biology, Department of Oncology, KU Leuven, 3000, Leuven, Belgium*
[i] *Trace, LKI Leuven Cancer Institute, KU Leuven, 3000, Leuven, Belgium*
[j] *School of Biomedicine, Far Eastern Federal University, 690922, Vladivostok, Russia*
[k] *Istituto di Scienze e Tecnologie Chimiche "Giulio Natta", Consiglio Nazonale delle Ricerche, 20131, Milano, Italy*

ARTICLE INFO

Article history:
Received 13 November 2020
Received in revised form
10 March 2021
Accepted 17 May 2021
Available online 30 May 2021

Keywords:
Wnt signaling
Triple-negative breast cancer
Clofazimine
Riminophenazine
Medicinal chemistry
Patient-derived xenograft

ABSTRACT

Triple-negative breast cancer (TNBC) is a cancer subtype critically dependent upon excessive activation of Wnt pathway. The anti-mycobacterial drug clofazimine is an efficient inhibitor of canonical Wnt signaling in TNBC, reducing tumor cell proliferation *in vitro* and in animal models. These properties make clofazimine a candidate to become first targeted therapy against TNBC. In this work, we optimized the clofazimine structure to enhance its water solubility and potency as a Wnt inhibitor. After extensive structure-activity relationships investigations, the riminophenazine 5-(4-(chlorophenyl)-3-((2-(piperazin-1-yl)ethyl)imino)-*N*-(pyridin-3-yl)-3,5-dihydrophenazin-2-amine **(MU17)** was identified as the new lead compound for the riminophenazine-based targeted therapy against TNBC and Wnt-dependent cancers. Compared to clofazimine, the water-soluble **MU17** displayed a 7-fold improved potency against Wnt signaling in TNBC cells resulting in on-target suppression of tumor growth in a patient-derived mouse model of TNBC. Moreover, allowing the administration of reduced yet effective dosages, **MU17** displayed no adverse effects, most notably no clofazimine-related skin coloration.

1. Introduction

Researchers and companies constantly seek novel strategies to reduce the costs and time investments of drug discovery and development. In this context, the use of an already approved drug for a new clinical indication represents an attractive approach. Unfortunately, it does not happen too often that an approved drug turns out to be perfect for the new clinical indication [1], which establishes the need for medicinal chemistry-based structural optimization to exalt the novel activity. Although the chemical

* Corresponding author. Department of Cell Physiology and Metabolism, Translational Research Centre in Oncohaematology, Faculty of Medicine, University of Geneva, 1206, Geneva, Switzerland.
** Corresponding author.
E-mail addresses: anna.sparatore@unimi.it (A. Sparatore), vladimir.katanaev@unige.ch (V.L. Katanaev).
[1] equally contributing as first authors.
[2] equally contributing as last authors.

https://doi.org/10.1016/j.ejmech.2021.113562

modifications introduced on the parent drug will require safety and efficacy reassessment in preclinical and clinical settings, the reuse of the data previously collected for the parental drug approval indeed provides a significant mitigation of risks and costs for the modified compound [2,3].

The Wnt pathway, a developmental signal transduction cascade controlling tissue growth, differentiation and patterning [4,5], is frequently switched on through mutational or epigenetic changes from its predominantly dormant state in healthy adult cells to drive cancer progression in organs such as breast, colon, liver, or ovaries [6–9]. Our previous studies identified the approved anti-mycobacterial drug clofazimine as a potent and specific inhibitor of the β-catenin-dependent canonical Wnt pathway and of the ensuing cell proliferation in triple-negative breast cancer (TNBC) *in vitro* and *in vivo,* providing the basis for the use of this drug against TNBC and other Wnt-dependent cancers [10–13]. Generally described as a highly lipophilic riminophenazine, clofazimine upon therapeutic administration accumulates in lipid-rich tissues, producing the most documented and psychologically harming side effect: the red skin-coloring [14–16]. Therefore, with the aim of developing novel clofazimine analogues endowed with the canonical Wnt signaling inhibitory activity in TNBC but possessing an improved safety profile, the current work provides a detailed medicinal chemistry investigation on the structure activity relationships of a panel of more than 40 riminophenazines structurally related to clofazimine (Tables 1 and 2). The compounds were tested *in vitro* for the inhibition of canonical Wnt signaling and for aspecific cytotoxicity, focusing on the effects of different tertiary amines as basic heads (introduced as a water-solubilizer at physiological pH in place of the original isopropyl group on the imino nitrogen of clofazimine), as well as of the concomitant modification of clofazimine's aromatic core by the replacement of the original C-3 *p*-chlorophenylamine moiety with a more hydrophilic pyridin-3-amine. These analogues were either previously described by us in the quest for novel anti-tuberculosis and antiprotozoal drugs [17,18] or *ad hoc* prepared for this study.

Some of the novel and most hydrophilic compounds, characterized by a C-3 aminopyridinyl riminophenazine core, showed up to a 7-fold improved potency against the Wnt pathway in TNBC cells as compared with the parent clofazimine, matched with an outstanding water-solubility, exceeding 0.1 M for some of the most potent (Supporting Table S1) - as compared to essential water insolubility of clofazimine. This dramatic improvement in the aqueous solubility strongly reduces deposition of the compound in subcutaneous fat and the consequent skin pigmentation. Moreover, the *in vitro* and *in vivo* pharmacodynamic profiles of the best performing compound **MU17** were found to outperform those of clofazimine. Thus, our study discloses strong improvement of the clofazimine scaffold for the specific anti-Wnt and anti-cancer treatment with reduced side effects in animals.

2. Results

2.1. SV12 and GG08: from an increase in aqueous solubility to improved anti-TNBC properties in vitro

Our investigation started with the *in vitro* evaluation of the ability to suppress the canonical Wnt activity by a family of riminophenazines, formally derived from clofazimine, bearing tertiary amines as polar, hydrophilic decorations connected with the aromatic core *via* alkyl linker of different lengths (compounds of Table 1). To this purpose, we used the Wnt3a-activated TopFlash reporter in the TNBC BT-20 cell line. Simultaneously, the unspecific/cytotoxic activity of the compounds was readout with the constitutively expressed CMV-Renilla luciferase. With exception of the new derivative **EB05(25)**, all the tested riminophenazines had previously been reported and analyzed in our studies on the compounds' anti-mycobacterial [19] or antiplasmodial and leishmanicidal activities [17,18]. In the current work, we additionally tested some synthetic intermediates (*i.e.* **SV05 (1)**, **SV01 (12)** and **INT262 (27)**). Results of the compounds' anti-Wnt activities are summarized in Table 1, which also provides the calculated selectivity index (S.I.) of each compound, defined as the ratio between the IC_{50} on the inhibition of the constitutively expressed Renilla luciferase and that of the Wnt-specific (TopFlash) IC_{50}, the former being indicative of the compounds' aspecific toxicity.

It can be stated that in our analysis of the effects of introduction of different basic heads and aromatic substituents with the respect of the original structure of clofazimine, a broad investigation of the chemical space has been achieved.

We experimentally validated aqueous solubility of basic clofazimine derivatives characterized by an aminophenyl group in position C-3 (**GM05**, **SV06**, **SV12**, **SV13** and **SV21**; **GM05**; **EB04** and **EB06**, Supporting Table S1). This property was found to be improved in comparison to clofazimine, agreeing with our expectations given the structural features of the derivatives. The most water-soluble compound of this series was the dimethylamine derivative **EB04**.

Compounds from **2** to **10**, which conserve the exact aromatic substituents of clofazimine and are characterized by the insertion of bicyclic (e.g. quinolizidine or pyrrolizidine moieties) or acyclic aliphatic tertiary amines, were found to be mostly inactive against the Wnt pathway, with the exception of 2-(hexahydro-1H-pyrrolizin-7a-yl)ethanaminyl and N^1,N^1-dimethylpropane-1,3-diaminyl derivatives **SV13 (9)** and **EB06 (10)**, which showed micromolar activities but comparable toxicities.

The fluorine derivatives **GM07 (11)** and **GM06 (12)**, instead, were totally inactive.

The Wnt-specific activity of compounds from **13** to **25**, whose lipophilia were further reduced by the removal of the two chlorine substituents of clofazimine, was strongly modulated by the nature of the basic head inserted in the commune aromatic core. Some derivatives (**15**–**17**, **19**, **20** and **24**) showed no inhibitory activity against the Wnt pathway and, in general, a neglectable cytotoxicity; others instead were able to strongly inhibit the pathway with different toxicities. The most interesting compound of this series, **SV12 (21)**, inhibited the Wnt pathway in the low-micromolar range with the S.I. of ~2.1.

Interestingly, among compounds **28**–**32** all bearing the C-3 aminopyridinyl moiety, **GG08 (32)**, one of the most hydrophilic compounds of Table 1, showed a micromolar Wnt-specific activity ($IC_{50} = 7.3$ μM) with the S.I. of *ca.* 2.2. To be noted that compounds **1**, **13**, and **28**, all lacking a C-2 basic side chain, were devoid of any Wnt-inhibitory activity.

The two most active and selective compounds **GG08** and **SV12** showed similar or slightly improved potency as compared to clofazimine. However, their *in vitro* specificity window, as showed by Fig. 1A, was reduced due to an overall increase of inhibition of the Renilla luciferase. Nonetheless, when analyzed for their ability to inhibit growth of TNBC cell lines, **SV12** and **GG08** outperformed clofazimine both in the MTT survival assay (Fig. 1B) and in the colony formation assay (Fig. 1C and D). In analogy with clofazimine and as expected from a compound affecting the canonical rather than non-canonical Wnt pathway [10,11], **SV12** and **GG08** demonstrated low or no inhibition of the ability of different cancer cells to migrate, with the notable exceptions of the MDA-MB-231 and MDA-MB-468 TNBC lines (Fig. 1E and F).

Table 1
Structures of the first family of clofazimine analogues tested and their respective Wnt-inhibitory activity, aspecific cytotoxicity and selectivity indexes.

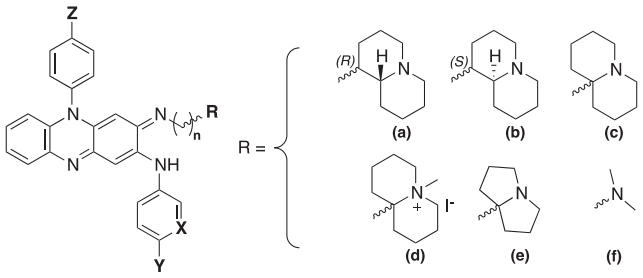

Label	Compound	X	Y	Z	n	R	Wnt-Inhibitory Activity IC_{50} (μM)	Aspecific Cytotoxicity IC_{50} (μM)	S.I.[a]
Clofazimine		CH	Cl	Cl	0	$CH(CH_3)_2$	7.2 ± 0.5	19 ± 1	2.6
SV05	**1**	CH	Cl	Cl	0	H	N.A.[b]	21.5 ± 8.9	N.D.[c]
CL-4	**2**	CH	Cl	Cl	1	a	N.A.[b]	24.3 ± 14.6	N.D.[c]
CL-5	**3**	CH	Cl	Cl	2	a	N.A.[b]	~95[d]	N.D.[c]
CL-6	**4**	CH	Cl	Cl	3	a	N.A.[b]	~8[d]	N.D.[c]
CL-11	**5**	CH	Cl	Cl	1	b	N.A.[b]	~73[d]	N.D.[c]
CL-12	**6**	CH	Cl	Cl	2	b	153.5 ± 108.8	>200	>1.3
CL-13	**7**	CH	Cl	Cl	3	b	N.A.[b]	~82[d]	N.D.[c]
SV06	**8**	CH	Cl	Cl	1	e	N.A.[b]	~100	N.D.[c]
SV13	**9**	CH	Cl	Cl	2	e	5.1 ± 1.9	8.0 ± 1.1	1.6
EB06	**10**	CH	Cl	Cl	3	f	2.8 ± 0.7	2.2 ± 0.1	0.8
GM07	**11**	CH	F	F	4	c	N.A.[b]	14.5 ± 1.5	N.D.[c]
GM06	**12**	CH	F	F	6	c	N.A.[b]	~11[d]	N.D.[c]
SV01	**13**	CH	H	H	0	H	N.A.[b]	~82[d]	N.D.[c]
CL-1	**14**	CH	H	H	1	a	21.9 ± 3.1	27.8 ± 2.6	1.3
CL-2	**15**	CH	H	H	2	a	N.A.[b]	15.8 ± 8.2	N.D.[c]
CL-3	**16**	CH	H	H	3	a	N.A.[b]	~33[d]	N.D.[c]
CL-8	**17**	CH	H	H	1	b	N.A.[b]	~36[d]	N.D.[c]
CL-9	**18**	CH	H	H	2	b	28.8 ± 5.4	29.9 ± 8.0	1.3
CL-10	**19**	CH	H	H	3	b	N.A.[b]	46.5 ± 8.4	N.D.[c]
SV02	**20**	CH	H	H	1	e	N.A.[b]	~50[d]	N.D.[c]
SV12	**21**	CH	H	H	2	e	6.3 ± 0.9	13 ± 1	2.1
GM05	**22**	CH	H	H	4	c	13.9 ± 1.9	17.5 ± 3.4	1.3
GM10	**23**	CH	H	H	4	d	98.6 ± 10.3	>100	>1.0
GM02	**24**	CH	H	H	6	c	N.A.[b]	~7[d]	N.D.[c]
EB05	**25**	CH	H	H	3	f	1.2 ± 0.1	1.6 ± 0.2	1.4
SV21	**26**	CH	CH_3	CH_3	1	a	N.A.[b]	~40[d]	N.D.[c]
EB04	**27**	CH	H	Cl	3	f	5.7 ± 0.8	5.4 ± 0.3	1.0
INT262	**28**	N	H	Cl	0	H	N.A.[b]	~42[d]	N.D.[c]
GG09	**29**	N	H	Cl	4	c	N.A.[b]	~35[d]	N.D.[c]
GG12	**30**	N	H	H	4	c	N.A.[b]	~11[d]	N.D.[c]
GG13	**31**	N	OCH_3	H	4	c	26.8 ± 1.0	39.2 ± 13.7	1.5
GG08	**32**	N	H	Cl	3	f	7.3 ± 1.8	16 ± 1	2.2

[a] S.I.: selectivity index is calculated as a ratio of IC_{50}s for aspecific cytotoxicity and Wnt Inhibition.
[b] N.A.: not active, specific anti-Wnt activity was not appreciable up to a 200 μM concentration.
[c] N.D.: not defined.
[d] IC_{50} was estimated through linear interpolation.

2.2. Wnt selectivity correlates with the alkyl spacer length of the C-2 side chain

Encouraged by these findings and intrigued by the possibility of developing highly hydrophilic riminophenazine-based clofazimine analogues endowed with potentialities as canonical Wnt-specific chemotherapeutic agents, a family of C-3 aminopyridinyl derivatives of **GG08**, bearing different basic heads connected to the aromatic nucleus with alkyl chains of different length, was designed, prepared and tested for its *in vitro* activity towards the Wnt pathway (Table 2). These compounds, with the exception of **AR18 (44)** and **AR13 (45)**, had been previously tested by us for their antiprotozoal activity [18].

We assessed the solubility of all the pyridine-containing basic riminophenazines of our study (**GG08** and **GG13**, **MU05**, **MU17** and **MU23**; **AR13** and **AR18**, Supporting Table S1). They were all found to be highly water soluble with solubility values $\geq$ 0.1 M. For example, when compared to clofazimine, **MU17** solubility in water was increased at least by a factor of ~10^5.

The results reported in Table 2 and Fig. 2A show that not only the nature of the basic head but also the length of the alkyl spacer plays a role in the Wnt pathway inhibition. In general, most compounds bearing butylene (**34**) or propylene-diamine (**36**, **38**, **40**, **42**) side chains inhibited the Wnt pathway more potently than the corresponding ethylendiamine derivatives (**33**, **35**, **37**, **39, 41**). Although the aspecific toxicity increased as well, the selectivity indexes, with the exception of the morfolinyl and *N*-methylpiperazinyl derivatives, improved in the compounds bearing longer alkyl spacers. On the contrary, the ethylenediamine-spaced *N*-methylpiperazinyl derivative **MU17** exhibited a *ca.* 2-fold better potency and a significantly higher S.I. than the two homologous **AR18** (**44**) and **AR13** (**45**) due to the reduction of the aspecific toxicity (Fig. 2B).

It can be argued that an "optimal linker length" is needed to produce Wnt-selective C3-pyridinyl basic riminophenazines and

Table 2
Structures and *in vitro* screening of the second-generation C-3 aminopyridinyl clofazimine analogues prepared and tested.

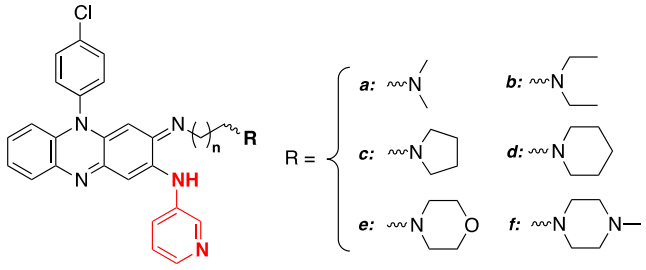

Label	Compound	n	R	Wnt-Inhibitory Activity IC_{50} (μM)	Aspecific Cytotoxicity IC_{50} (μM)	S.I.[a]
MU12	**33**	1	a	3.50 ± 0.30	2.83 ± 0.21	0.8
MU21	**34**	3	a	0.86 ± .06	1.24 ± 0.08	1.4
EB01	**35**	1	b	6.28 ± 0.62	5.92 ± 0.68	0.9
MU05	**36**	2	b	1.60 ± 0.34	3.96 ± 0.30	2.5
MU09	**37**	1	c	1.75 ± 0.26	2.3 ± 0.26	1.3
MU23	**38**	2	c	0.87 ± 0.19	1.96 ± 0.08	2.3
MU10	**39**	1	d	2.15 ± 2.05	2.37 ± 0.18	1.1
MU24	**40**	2	d	1.38 ± 0.07	1.93 ± 0.08	1.4
MU25	**41**	1	e	10.62 ± 1.83	7.88 ± 3.37	0.7
MU15	**42**	2	e	5.13 ± 0.57	2.83 ± 0.21	0.6
MU17	**43**	1	f	1.1 ± 0.1	2.7 ± 0.2	2.5
AR18	**44**	2	f	3.0 ± 0.5	5.1 ± 0.5	1.7
AR13	**45**	3	f	2.5 ± 0.2	4.5 ± 0.4	1.8

[a] S.I.: selectivity index is calculated as a ratio of IC_{50}s for aspecific cytotoxicity and Wnt Inhibition.

also that this optimum is related to the nature of the amine head. For the flexible and conformationally-free diethylamine and dimethylamine derivatives (compounds **GG08** and **33**–**36**), in fact, a propylendiamine-spaced linker ensures S.I. > 2. The same trend was instead not seen in relation with the more sterically demanding piperidine and morpholine derivatives (compounds **39**–**42**) whose selectivity appeared to be less or not at all sensitive to the length of the alkyl linker. At variance, the pyrrolidinyl derivatives **37**–**38** were perfectly aligned with compounds **33**–**36**.

The case of the *N*-methyl piperazinyl derivatives is by far the most interesting, since the most selective derivative of the series, **MU17 (43)**, contains the ethylenediamine linker.

To further investigate these results, we conducted a ligand overlay-based conformational analysis of all the C-3 pyridinyl derivatives of Tables 1 and 2 using the Hermes module of the CCDC-suite (ccdc.cam.ac.uk/) to investigate the conformational space allowed to over-impose their most energetically favorable conformer [20,21]. The CCDC suite was also used to generate a putative and preliminary pharmacophore model by superposing a set of active molecules assuming binding to the same target with the same binding mode, as we previously reported for a panel of potent but target-less antiprotozoal agents [22]. Fig. 3 summarizes the obtained results.

As a representative example, the conformational overlay (Fig. 3, *left*) of the selective and potent compounds **MU17** (black) and **GG08** (gray) with the least selective of the group, **MU15 (42)** (blue), shows how the positively-charged nitrogens of the former two are positioned in the same area and are mostly overlaid. The same was not found for the oxygen-containing morpholinyl-derivative **MU15 (42)** whose charged group orientation and alkyl chain folding appear quite different, according to its different biological profile. On the basis of the ligand overlay experiment conducted (for details see the Experimental Section), a pharmacophore model of the most selective C-3 aminopyridinyl compounds **MU17** and **GG08** was also created using their calculated surfaces of interaction. This model further highlighted the presence of a highly directional donor-surface (blue in Fig. 3, *right*) generated from the positively charged nitrogen of the solubilizing basic heads of the two compounds which could be involved in the interaction with a still-unidentified protein target within the Wnt pathway.

2.3. Administration of MU17 significantly inhibits TNBC tumor growth in vivo

We have next analyzed the ability of the most selective and potent hydrophilic riminophenazine **MU17** to inhibit tumor growth in the patient-derived xenograft (PDX) model of triple-negative breast cancer (TNBC) BRC0016. Since the solubilizing moiety, *i.e.* the basic *N*-methylpiperazine head, would likely restrict oral bioavailability [23] we decided to deliver the compound by intraperitoneal injections at 20 mg/kg daily. As shown in Fig. 4 (A-D), this treatment for a group of 3 mice alongside with the equal control group over 21 days resulted in a significant decrease in the tumor volume without incurring any changes on the body weight of the animals or affecting any other thoroughly controlled parameters of the animal well-being, such as urine and faeces conditions or overt behavior and pain signs, indicating the safety of the new compound. Additionally, we analyzed levels of **MU17** at different doses and treatment durations in the liver and inside the tumors (Fig. 4E). The presence of **MU17** in blood was also investigated at different post-injection (3h and 24h) times revealing that, despite its impressive aqueous solubility, the compound was virtually absent in the blood samples showing only non-quantitative trace signals (data not shown). However, **MU17** was clearly progressively accumulated in the tumors eventually reaching values well above the IC_{50} observed for the Wnt pathway inhibition *in vitro*. The compound levels in liver might provide an explanation why **MU17** was not found in blood: **MU17** seems to be strongly retained by this organ and thus likely to be susceptible to hepatic clearance. These findings are also compatible with the absence of detectable compound levels in the faeces and urine (not shown). Interestingly, one consequence of the significantly

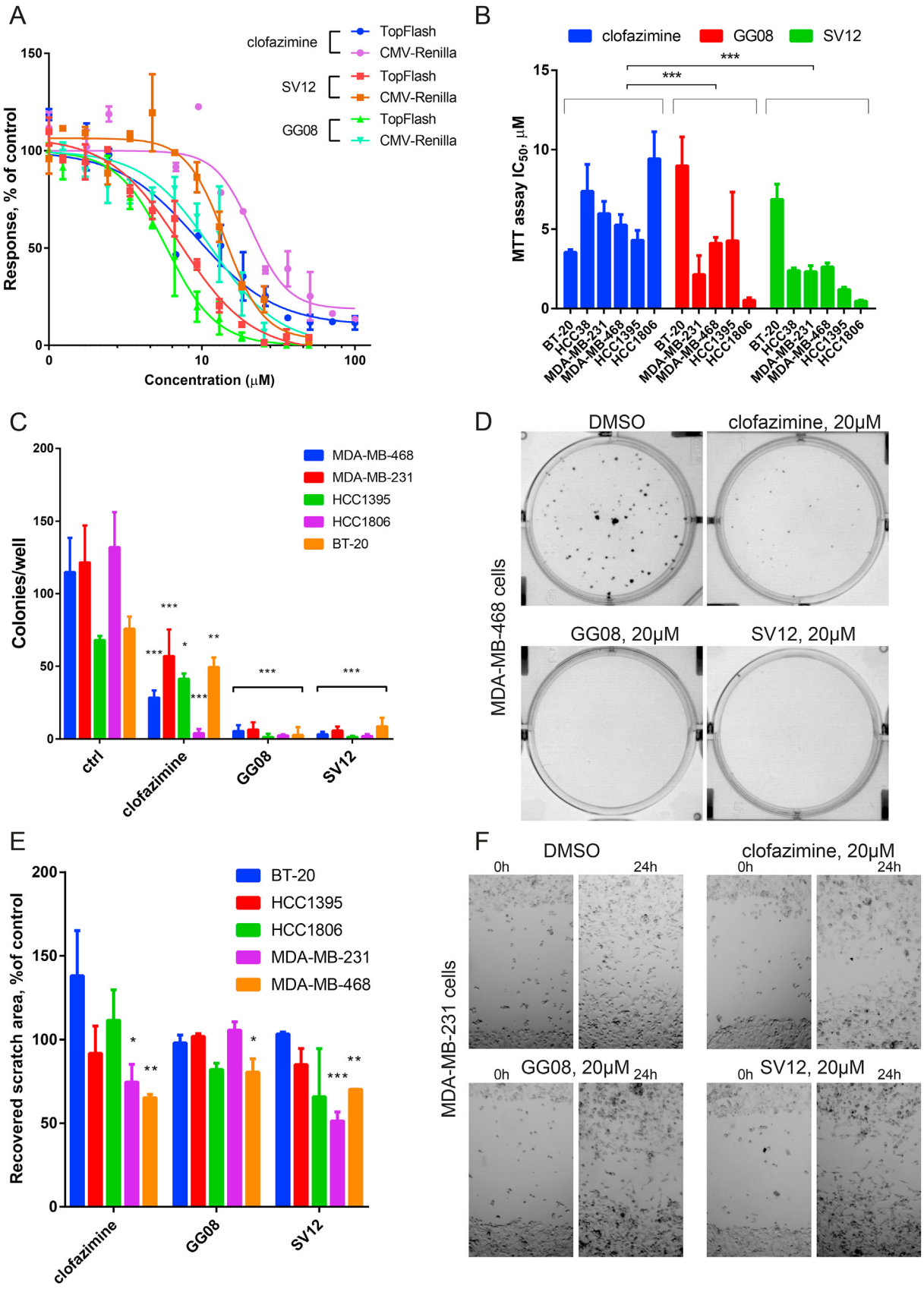

Fig. 1. Clofazimine derivatives **GG08** and **SV12** show inhibition of the canonical Wnt signaling and anti-cancer properties similar to the parental drug. **(A)** Activity of these derivatives was tested in the Wnt3a-induced TopFlash assay with constitutively expressed CMV-Renilla luciferase as a non-specific inhibition and cell toxicity readout. **(B)** Both compounds are also capable of inhibition of growth in the panel of TNBC cell lines, showing overall improved potency as compared to clofazimine. **(C, D)** Similarly, the compounds (all at 20 μM) successfully inhibit growth of the cancer cells in colonies, showing higher efficacy as compared to clofazimine – likely due to the improved solubility, since

increased aqueous solubility of **MU17**, when compared to clofazimine, was the absence of the skin coloration during the trials – the feature readily observed when mice are treated with the parental compound (Fig. 4F).

2.4. MU17 maintains the on-target anti-Wnt effect in vivo

Using the extracted tumors, we were also able to confirm through the immunofluorescence analysis the on-target effect of **MU17** *in vivo*. As shown in Fig. 5A, the animal treatment with the compound resulted in significant changes in the tumor β-catenin pattern, reducing the number of cells with cytoplasmic staining of this major Wnt signaling biomarker. This hallmark of Wnt signaling reduction in the breast cancers [24] correlated with decrease in the proliferation marker Ki67 staining and the corresponding increase in the number of apoptotic cells highlighted by expression of caspase-3 (Fig. 5B and quantification on **5C**).

2.5. MU17 targets nuclear components of the canonical Wnt signaling pathway

As we reported earlier [10,11], clofazimine inhibits canonical Wnt signaling below the level of β-catenin, thus likely targeting one of the multiple components of the pathway within cell nucleus. We thus investigated if **MU17** maintains the same mode of action and confirmed that **MU17**, just like clofazimine [10], is highly specific towards Wnt signaling. First, we verified that **MU17** and the other potent riminophenazines **GG08**, **SV12**, **AR18** and **AR13** do not reveal inhibition in the FopFlash assay, which employs a reporter plasmid similar to TopFlash but with the mutated TCF binding site (Supporting Fig. S1A). Further, we profiled **MU17** and the listed compounds against a panel of luciferase reporters for different signaling pathways (Supporting Fig. S1B), detecting no inhibition against any of them.

In order to further assess the mechanism of action of the clofazimine compounds, we tested if and at which time point **MU17** could affect cellular β-catenin. We probed for the levels of active β-catenin in BT20 and MDA-MB-468 cells (Fig. 6A, B) at 5h and 24h of treatment with the compound. Similarly to clofazimine [11], **MU17** was unable to acutely suppress levels of the active β-catenin in 5h – agreeing with the findings above that suggested that the drug acted below β-catenin. To further corroborate these findings, immunostaining of total β-catenin and phospho-β-catenin (pS33/37/T41-β-catenin, indicative of the protein targeted for proteasomal degradation) in the same cells stimulated by Wnt3a and treated with **MU17** for 5h shows that the drug is unable to acutely influence the Wnt3a-induced decrease in phospho-β-catenin nor the total β-catenin nucleocytoplasmic accumulation (Fig. 6C, D, E). Curiously, a strong suppression of β-catenin levels is evident upon the prolonged 24h treatment with **MU17** (Fig. 6A, B), agreeing with our previous findings *in vitro* and *in vivo* with clofazimine [10], and our current *in vivo* findings with **MU17** (Fig. 5A). Thus, we conclude that the direct molecular target of action of clofazimine and its derivatives in the Wnt pathway is below nuclear translocation of β-catenin. However, the prolonged inhibition of this target likely engages a positive feedback loop, since a number of Wnt pathway target genes are also pathway components (e.g. FZD7, Wnt3a) [6], which further induces a decrease in the cytonuclear β-catenin levels. Future research will identify the nuclear Wnt pathway target of clofazimine with the network properties so promising in terms of the efficient and double-edged inhibition in TNBC.

3. Discussion and conclusions

Even among the approved modern drugs, only few compounds can boast with their absolute selectivity towards the desired target. Depending on the exact methods and cutoffs used for estimates, many of the approved drugs are known to have between 1 and 10 off-target interactions in addition to its target protein [25–27]. Often left unknown and being generally undesirable due to the ensuing potential adverse effects, these interactions might also turn out as a surprising asset when leading to a new medical indication. In this case, decades of prior research on the pharmacokinetics and safety profile of the drug might lead to multi-million R&D cost and risk mitigation along with a fast-track development for the new indication [28].

This work represents a next step in our quest to transform the clofazimine scaffold into a Wnt-targeting anti-cancer chemotherapeutic agent [10–12]. While this compound by itself shows an excellent anti-TNBC activity both *in vitro* and *in vivo*, no attempts were undertaken so far to improve its anti-Wnt properties through medicinal chemistry optimization: after the development in 1950s [29], the full potentialities of the riminophenazine skeleton of clofazimine have not yet been fully explored by means of modern chemistry and molecular biology. In a wake of multidrug-resistant strains of *Mycobacterium tuberculosis*, attempts to close this gap are already ongoing by the preparation of more hydrophilic clofazimine analogues as anti-tuberculosis agents [19,30].

Thus, we decided to apply a similar approach by *in vitro* screening of a collection of hydrophilic clofazimine analogues decorated with tertiary amines as basic heads [17–19] as a starting point to develop water-soluble derivatives endowed with the specific anti-Wnt activity. As expected, given the broad range of biological activities showed by riminophenazines and the fact that compounds of Table 1 were designed to be anti-tuberculosis and antiprotozoal agents, only a handful of the derivatives was able to efficiently and specifically inhibit the Wnt pathway. However, two of them – **SV12** and **GG08** – were able to suppress Wnt signaling with a potency similar to that of clofazimine. This result indicates that the addition of tertiary amines as basic heads, which can act as water-solubilizing groups, did not harm the clofazimine activity. These experiments also provided valuable information about the possible modifications of the clofazimine scaffold in view of obtaining the Wnt-specific inhibitors. Indeed, introduction of a C3-aminopyridinyl substituent, of a highly flexible alkyl chain and of a hydrophilic dimethyl amine boosted the compound selectivity, potency and water solubility.

On the basis of these encouraging results, a second generation of C3-aminopyridinyl basic clofazimine analogues structurally related to **GG08**, also previously tested by us for their antiprotozoal activity [18] was screened *in vitro* for the anti-Wnt activities (Table 2). The potent *N*-methyl piperazinyl-based **MU17**, characterized by an ethylenediamine linker resulted to be optimal for boosting the selectivity of the Wnt pathway inhibition of the series of piperazinyl derivatives (compounds **43**–**45** in Table 2), was identified as a prime candidate for further *in vivo* investigation in mice bearing patient-derived TNBC xenografts. Accordingly, **MU17** showed a 7-fold improvement in the anti-Wnt IC_{50} when compared to clofazimine while its selectivity index remained at the 2.5-fold level, similar to that of parental clofazimine. It is thus reasonable to

clofazimine is known to eventually precipitate from the culture medium. **(E, F)** Both clofazimine and the **GG08** and **SV12** derivatives (all at 20 μM) have little or no activity in inhibiting cancer cell migration in scratch-wound assay, with MDA-MB-231 and MDA-MB-468 cell lines as exceptions. Statistical significance was assessed by two-way ANOVA with multiple comparisons for main effect per compound (panel A) or individually for each line (panels C and E), N = 3, significance is shown as *p < 0.05, **p < 0.01 and ***p < 0.001.

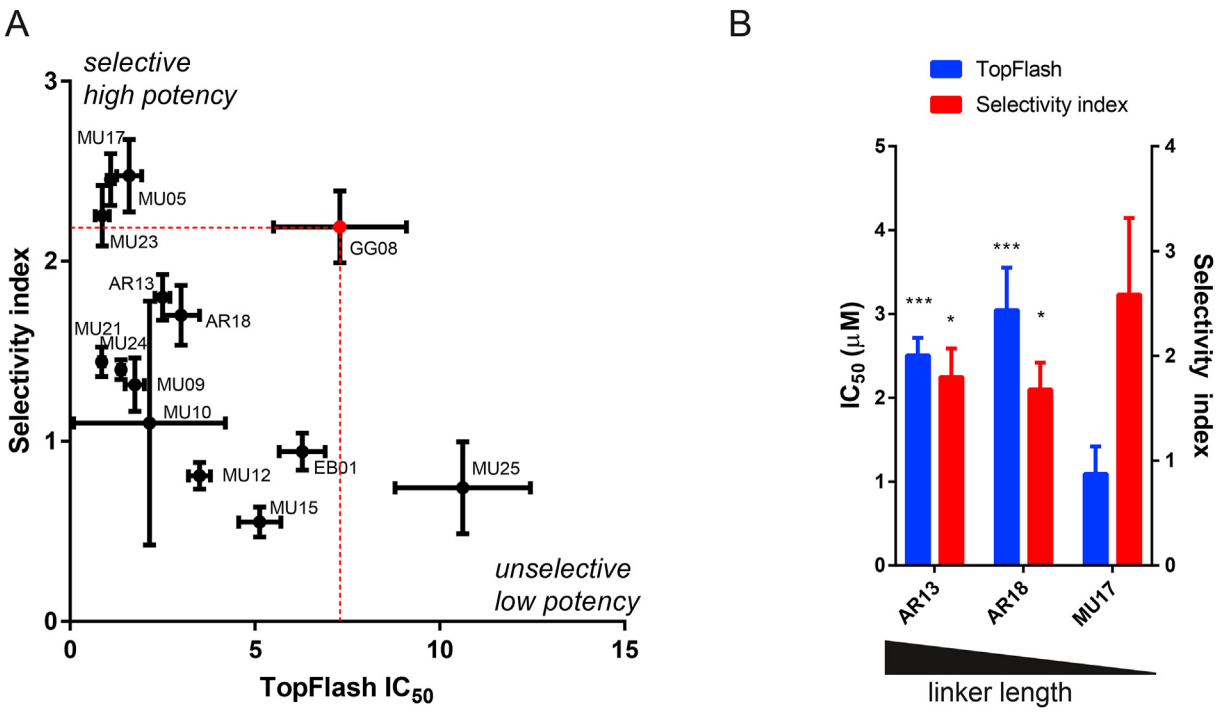

Fig. 2. (A) Correlation between the Wnt-specific activity (TopFlash IC_{50}) and selectivity of the hydrophilic derivatives of **GG08** (Table 2). In respect to **GG08**, most of the compounds were found to clusterize in the bottom-left section of the chart as their potency was improved by the structural changes but their selectivities were concomitantly reduced. **MU23**, **MU05** and **MU17** instead grouped in the upper-left section of the chart in which compounds with improved potency and selectivity with the respect to **GG08** are clusterized. Only one of the novel derivatives (**MU25**) was less potent and less selective than **GG08**. (B) Variation of the linker length among **AR13**, **AR18**, and **MU17**, shows that 2 methylenes of **MU17** are optimal due to reduced cytotoxic activity. Statistical significance was assessed by two-way ANOVA with multiple comparisons. N = 4, significance is shown as on Fig. 1.

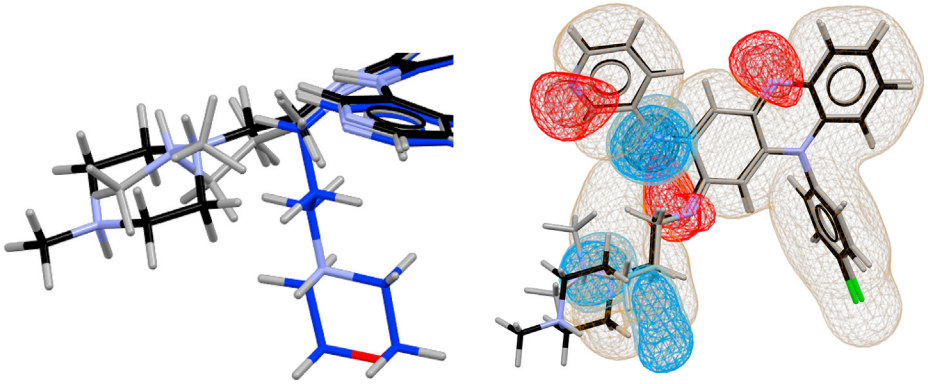

Fig. 3. *Left*) *In silico* section of the conformational overlay of **MU17** (black), **GG08** (gray) and **MU15(42)** (blue); *Right*) pharmacophore mapping of **MU17** (black) and **GG08** (gray): in red, blue and yellow are highlighted the areas in which acceptor, donor and non-polar interactions can be established, respectively.

suggest that the selection of a proper linker length associated with the nature of the basic heads inserted onto the common aromatic riminophenazine core could affect the affinity of a tested analogue toward specific targets both within and outside the Wnt pathway explaining the lower S.I. characterizing some of our C3-pirydinyl riminophenazines as compared to **MU17**.

Comparably to clofazimine [10], **MU17** demonstrated a promising profile as potential chemotherapeutic agent in the model of highly aggressive grade III invasive ductal triple-negative adenocarcinoma, resulting in significant (3 to 4-fold) reduction in the tumor volume at a comparable dose of 20 mg/kg (clofazimine itself has shown profound effect at 25 mg/kg, as described by us [10]), delivered intraperitoneally. Also, **MU17** upon application to animals was found not to produce any obvious adverse effects. Importantly, the significantly increased solubility of this *N*-methylpiperazinyl analogue (>0.3 M) resulted in the absence of deposits in the subcutaneous adipose tissue, eliminating one of the formally harmless, reversible but most conspicuous adverse effects of the clofazimine administration, skin coloration – and this is despite the fact that the derivative maintains the strong red color characteristic of the scaffold. Moreover, we expect that this property might lead to drastic reduction of the other skin-related conditions known to be associated with clofazimine such as rash, dryness and ichtiosis [31,32].

Despite that **MU17** apparently loses the ability to accumulate in adipose tissues, the compound was still well-retained in the tumor resulting in a profound reduction of the in-tumor Wnt signaling levels, evaluated as loss of cytoplasmic β-catenin – a hallmark of

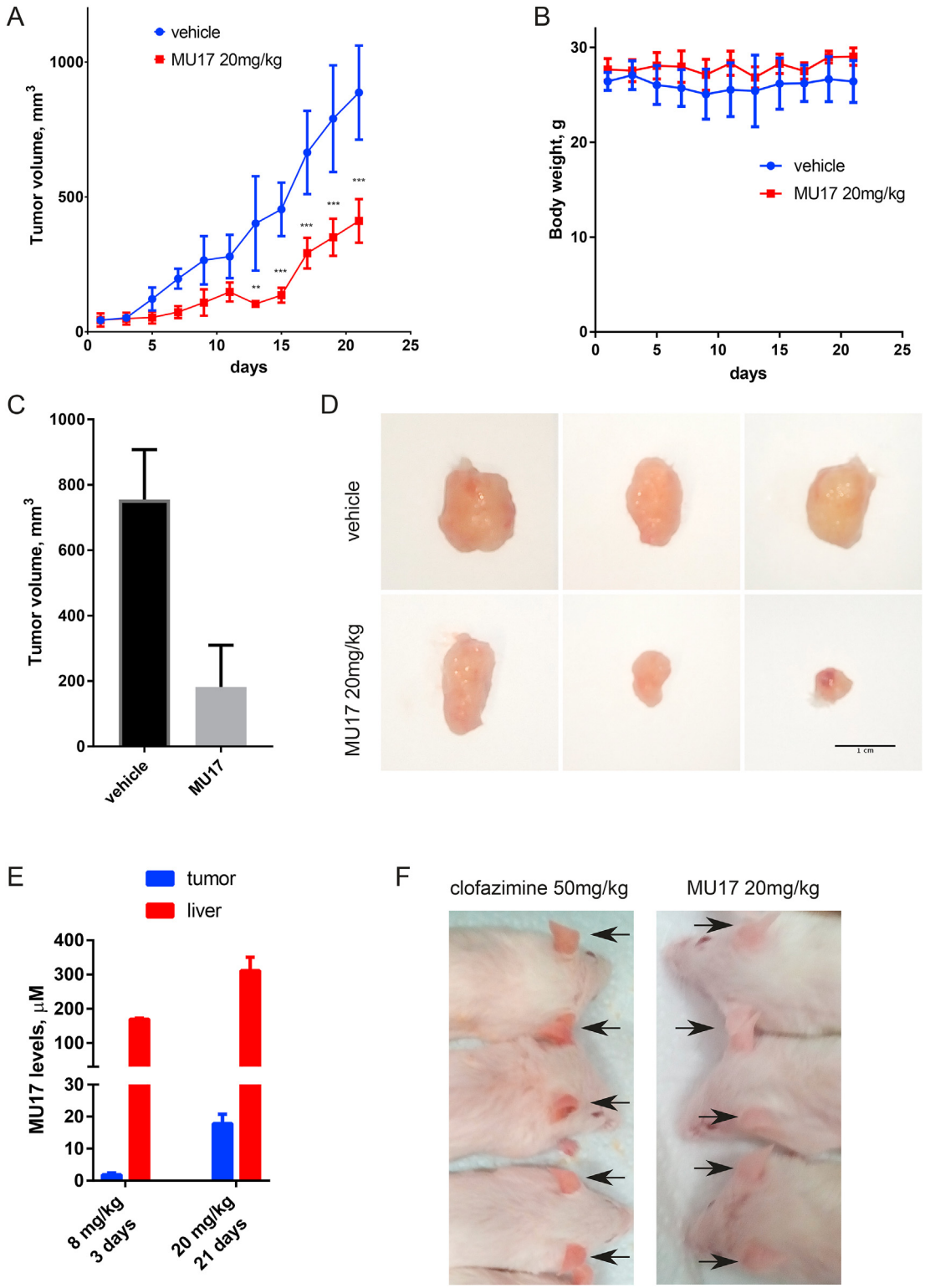

Fig. 4. Daily IP administration of 20 mg/kg **MU17** in mice bearing intramammary BRC0016 patient-derived TNBC xenografts results in significant reduction of the tumor volume as measured by electronic calipers **(A)**, without any effects on animal body weight **(B)**. **(C, D)** Endpoint analysis of the extracted tumors confirms results of the manual measurement. **(E)** Levels of **MU17** in the livers and tumors of the treated animals at different dosage and treatment duration indicate that at 20 mg/kg the compound reaches tumor levels well above IC_{50}. **(F)** Increased solubility of the compound results in reduction of subcutaneous deposition of the drug and thus absence of pigmentation in the treated animals. Each drug- or vehicle-receiving group consisted of N = 3 animals.

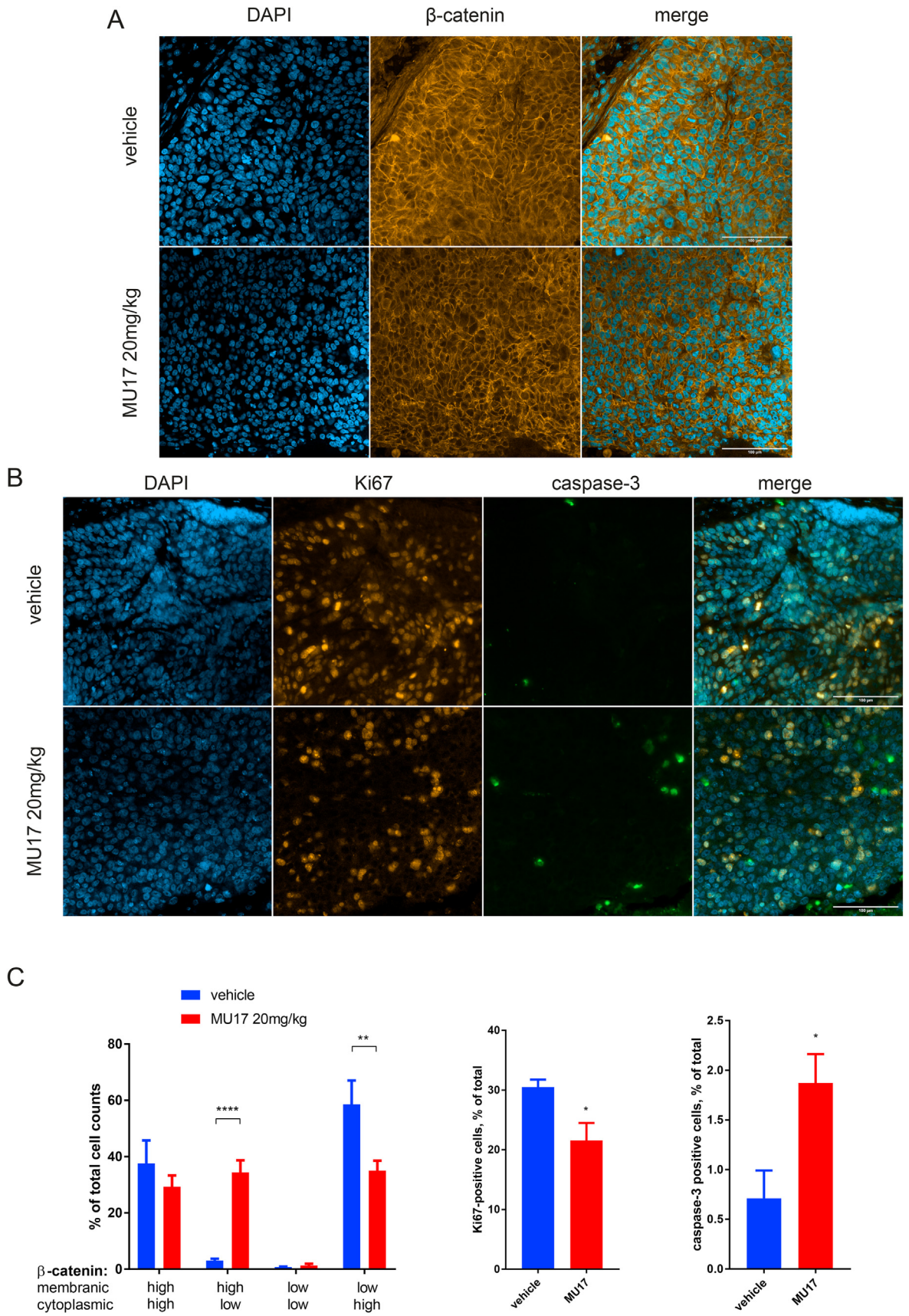

Fig. 5. MU17 confers on-target anti-Wnt effect of clofazimine *in vivo*. (A) Staining of the tumor sections shows a profound reduction in the cells positive for cytoplasmic β-catenin. (B) Additionally, when stained for Ki67 and caspase-3, the tumors show an increased number of apoptotic and a decreased number of proliferating cells. (C) Quantification of the effects of clofazimine on β-catenin. Each cell was assigned to one of the four types depending on the observed pattern of β-catenin localization. Cell counts reveal that **MU17**

the Wnt signaling activation in breast cancer [24], whose dramatic loss we have also observed during treatment with parental clofazimine [10]. The tumor proliferation marker Ki67 was also decreased, on the background of increased apoptosis. Despite this, the high levels of **MU17** found in the liver and its virtual absence in the blood indicate that this compound is overall strongly susceptible for hepatic clearance, although the metabolites have not yet been searched for. Further improvements on this aspect, along with more detailed *in vivo* pharmacokinetics studies, might in the future generate derivatives that could require less frequent dosage regimens with more steady levels reached in the tissues.

Overall, our study paves the way for the development of novel C3-aminopyridinyl riminophenazines structurally related to clofazimine with improved potency, much higher solubility and thus reduced skin deposition, with potential for future use as perfusion and subcutaneous or intramuscular injections and represent an important step towards development of novel targeted anti-cancer therapies based on the clofazimine scaffold.

4. Experimental Section

4.1. Synthetic chemistry

4.1.1. Material and methods

All commercially available solvents and reagents were used without further purification, unless otherwise stated.

NMR spectra were recorded on a Varian Mercury 300 VX spectrometer in $CDCl_3$, CD_3OD or DMSO-d_6 and chemical shifts were reported in ppm (δ). Peaks were assigned with 2D COSY experiments and are in agreement with the proposed structures.

TLC was carried out on Merck precoated 60 F254 plates using UV light and dipping with ethanol/phosphomolybdic acid 10% or a 10% w/v ethanolic solution of ninidrine.

Flash column chromatography was performed using silica gel 60 (0.040–0.063 mm, Merck).

Organic phases were dried over anhydrous sodium sulphate. Concentrations were performed under diminished pressure (1–2 kPa) at a bath temperature of 40 °C.

High-resolution mass spectra (HRMS) on FT-Orbitrap mass spectrometer in positive electrospray ionization (ESI).

Purities of final compounds described in the manuscript was >99% as determined by HPLC using CH_3CN/H_2O + CF_3COOH gradient and a Purospher RP18 5 μm column on a Hitachi Elite Lachrom Instrument equipped with a DAD detector. Rt. = retention time.

ATR-FT-IR spectra were recorded using an Alpha spectrometer equipped with an ALPHA's Platinum single reflection diamond ATR unit (Bruker Optics, Milan, Italy). Scans number n = 40. Instrumental resolution 5 cm^{-1}.

^1H NMR, ^{13}C NMR, HRMS and IR spectra of the novel compounds **EB05**, **AR18** and **AR13** are provided in the Supporting Information.

4.1.2. Previously reported compounds

Compounds from **1** (**SV05**) to **24** (**GM02**) and from **26** (**SV21**) to **32** (**GG08**) (Table 1) were prepared as we described [17,19]. All the compounds of Table 2, with the exception of **AR18** (**44**) and **AR13** (**45**), were instead synthetized as we previously reported [18].

4.1.3. Novel compounds: EB05 (25), AR18 (44) and AR13 (45)

The novel riminophenazines were obtained following Scheme 1 (**EB05** (**25**)) or Scheme 2 (**AR18** (**44**) and **AR13** (**45**)), depending on the structure of their riminophenazine core. In both cases, target products were obtained following the below reported general procedure for immination reaction (step ii in Scheme 1 and step iv in Scheme 2):

Under nitrogen atmosphere, the desired phenazine core (1 equiv.) and the proper N^1,N^1-substituted alkyl-diamine (2 equiv.) were dissolved in 1,4-dioxane ([phenazine] = 65 mM) and refluxed for 6 h. After cooling, the solvent was removed *in vacuo* and the obtained residue was diluted with dichloromethane (DCM) and washed three times with water. The organic layer was dried with anhydrous sodium sulphate and evaporated to dryness. The crude product was purified by flash column chromatography [gradient of methanol (MeOH) in DCM] and converted, using an excess of 1 M ethanolic solution of HCl, into the corresponding solid hydrochloric salt which was rinsed with diethyl ether. For NMR characterization the salts were converted again into the corresponding free bases.

EB05 (**25**) (isolated yield: 60%, HPLC purity > 99%) was obtained by reacting N^1,N^1-dimethylpropane-1,3-diamine with the phenazine core 3-imino-*N*,5-diphenyl-3,5,10,10a-tetrahydrophenazin-2-amine prepared by the oxidation of the corresponding N^1-phenylbenzene-1,2-diamine with ferric chloride [29]. Compound eluates from the flash column chromatography with the 5% of MeOH in DCM.

^1H NMR (300 MHz, $CDCl_3$, r.t.), δ: 7.76–7.66 (m, 4H), 7.39–7.33 (m, 5H), 7.23–7.09 (m, 3H), 6.99 (s, 1H), 6.53 (d, J = 8.0 Hz, 1H), 5.34 (s, 1H), 3.17 (t, J = 6.8 Hz, 2H), 2.34 (t, J = 7.5 Hz, 2H), 2.21 (s, 6H), 1.81 (quintet, J = 7.2 Hz, 3H).

^{13}C NMR (75 MHz, CD_3OD, r.t.), δ: 152.5, 145.5, 141.4, 139.6, 139.2, 136.1, 135.8, 132.2, 131.45, 131.37, 130.3, 129.5, 127.8, 127.4, 124.9, 122.4, 117.2, 105.9, 90.3, 55.2, 42.3, 41.1, 22.5.

HRMS (ESI) *m/z* calcd for $C_{29}H_{30}N_5$ $[M+H]^+$: 448.2501, found: 448.2506.

AR18 (**44**) (isolated yield: 30%, HPLC purity > 99%) was obtained by reacting 3-(4-methylpiperazin-1-yl)propan-1-amine, prepared as reported [33], with the phenazine core 5-(4-chlorophenyl)-3-imino-*N*-(pyridin-3-yl)-3,5,10,10a-tetrahydrophenazin-2-amine obtained from commercially available N^1-(4-chlorophenyl)benzene-1,2-diamine, 1,5-difluoro-2,4-dinitrobenzene and pyridine-3-amine *via* a series of nucleophilic aromatic substitutions, reduction and oxidative intramolecular cyclization [17,18,29]. Compound eluates from the flash column chromatography with the 10% of MeOH in DCM.

^1H NMR (300 MHz, CD_3OD, r.t.), δ: 8.42 (d, J = 7.3 Hz, 1H), 8.31 (d, J = 6.1 Hz, 1H), 7.96–7.81 (m, 5H), 7.69–7.62 (m, 4H), 7.22 (d, J = 7.2 Hz, 1H), 6.01 (s, 1H), 3.62–3.46 (m, 10H), 2.94–2.91 (m, 5H), 2.18 (bs, 2H).

^{13}C NMR (75 MHz, CD_3OD, r.t.), δ: 161.2, 153.2, 145.0, 139.4, 137.8, 136.4, 135.8, 134.4, 134.1, 133.4, 132.8, 131.9, 131.7, 131.0, 130.8, 129.4, 129.1, 128.2, 127.4, 117.1, 115.3, 90.7, 54.0, 50.7, 42.3, 41.1, 22.6.

HRMS (ESI) *m/z* calcd for $C_{31}H_{33}N_7Cl$ $[M+H]^+$: 538.2486, found: 538.2485.

AR13 (**45**) (isolated yield: 33%; HPLC purity > 99%) was instead obtained by reacting 3-(4-methylpiperazin-1-yl)buthyl-1-amine, prepared as reported [33] with the same phenazine core used for **AR18** (**44**). Compound eluates from the flash column chromatography with the 10% of MeOH in DCM.

^1H NMR (300 MHz, $CDCl_3$: CD_3OD = 8/2, r.t.), δ: 8.28 (s, 1H), 7.89 (s, 1H), 7.77–7.76 (m, 1H), 7.68–7.66 (m, 1H), 7.27–7.18 (m, 6H), 6.93–6.85 (m, 3H), 6.54–6.53 (bs, 1H), 5.30 (s, 1H), 3.01–2.99 (m,

treatment significantly enriches the proportion of cells with high membrane and low cytoplasmic β-catenin, while correspondingly decreasing the share of the cells positive for the cytoplasmic staining only. Statistical significance was assessed by two-way ANOVA (for membranic/cytoplasmic β-catenin quantification) or by Student's t-test. N = 3, *p* values are reported as on Fig. 1.

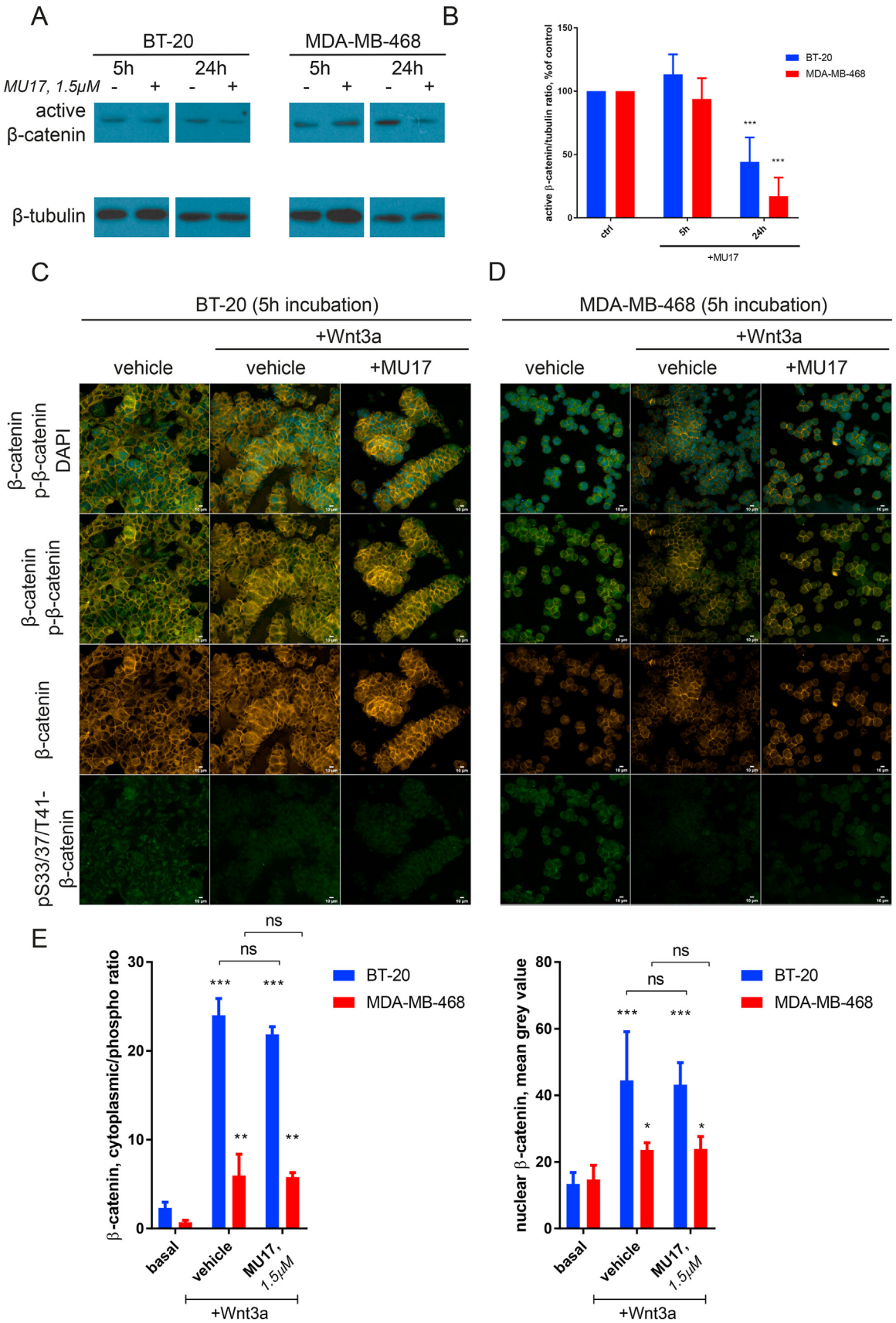

Fig. 6. MU17 maintains the mode of action of clofazimine and likely targets a nuclear component of the canonical Wnt signaling. (A,B) Analysis of active β-catenin in TNBC cell lines reveals no decrease of its levels in response to **MU17** in 5h; however, it does reduce these levels in 24h. (C, D) Immunostaining of total and phospho-β-catenin with quantifications of

6H), 2.72–2.64 (m, 6H), 2.31 (s, 3H), 1.38–1.36 (bs, 2H), 1.24 (bs, 2H).

^{13}C NMR (75 MHz, $CDCl_3$: CD_3OD = 8/2, r.t.), δ: 157.2, 148.9, 145.9, 143.1, 142.1, 141.6, 140.1, 139.0, 138.4, 137.7, 136.2, 135.0, 134.8, 132.9, 132.3, 131.6, 120.9, 118.4, 94.4, 67.1, 60.0, 47.5, 46.5, 33.4, 28.0, 25.3.

HRMS (ESI) *m/z* calcd for $C_{32}H_{35}N_7Cl$ $[M+H]^+$: 552.2642, found: 552.2640.

4.2. In silico calculations

Two clusters of compounds were identified from Table 2 on the basis of compounds selectivity for Wnt-inhibition: compounds with S.I. > 2.0 defined cluster A while compounds with S.I. < 2.0 defined cluster B. **GG08** was added to cluster A.

At first, compounds' structures were refined by assigning atomic types, adding a formal positive charge on the basic group of the solubilizing basic heads with the DiscoveryStudio and cleaned-up with a Dreeding-like force field. After that, the Mercury module of the CCDC-suite was used to generate 200 conformers for each compound which were used as the input of a ligand overlay-based pharmacophore modeling run with the Hermes module of the same suite. The obtained overlays were screened on the base of their internal energy and statistical relevance. Combining the data obtained from ligand overlay of the two clusters, a pharmacophore model was finally visualized as a surface-field representation.

4.3. Biological evaluation

4.3.1. Luciferase activity measurements

The Wnt-induced and basal luciferase activity was analyzed as described [11]. Briefly, 30 μl of BT-20 cells, wild type or stably transfected with the TopFlash luciferase reporter at 6000 cells/well were distributed in a white opaque 384-well plate. The cells were maintained in DMEM containing 10% FBS and incubated at 37 °C, 5% CO2 overnight for attachment. Afterwards, the stably transfected BT-20 cells were additionally transfected with the plasmid constitutively (under the CMV promoter) expressing Renilla luciferase (Addgene, Cambridge, MA, USA). Transfection was carried out as described in manufacturer's protocol using 12 μg/ml of DNA and 40 μl/ml XtremeGENE 9 reagent (Roche), 1 μl of the final mixture was subsequently added per well.

Next day, the medium of each well was replaced by 30 μl (384-well plates) fresh medium containing Wnt3a (500 ng/ml) (purified as described [34]) and compound concentrations indicated in the figures (following 1h of pre-incubation with the compound). After overnight incubation, the supernatant in each well was removed and the luciferase activity was measured in the Tecan Infinite 200 Pro reader.

4.3.2. MTT assay

50 μl of indicated TNBC cell lines were added into each well of a transparent 384-well plate at density 1500 cells/well. The cells were maintained in DMEM containing 10% FBS and incubated at 37 °C, 5% CO2 overnight. The next day, the medium of each well was replaced by 50 μl fresh medium containing indicated concentrations of compounds. After incubation for 3–4 days, the medium in each well was replaced by 50 μl of 0.5 mg/ml Thiazolyl blue (Carl Roth) solution in 1xPBS. The plates were incubated for 3h at 37 °C. Then the solution was removed, and 30 μl DMSO was added into each well. Absorbance at 570 nm was measured in the Tecan Infinite 200 Pro reader.

4.3.3. Scratch-wound and colony formation assays with TNBC cells

For migration analysis, the scratch-wound assay was used. Cells were seeded at 60′000 cells/well in 96-well flat-bottom plates. Next day, after attachment, the monolayer formed in each well was wounded in two places by a single strike of a 10 μl pipette tip. The detached cells were removed by 2x wash with 1xPBS. For each experimental well, a random area of both scratches was labeled and a phase-contrast picture was taken. The cells were left for 24h in presence or absence of indicated concentrations of tested compound. Afterwards, the pictures of the same area were taken and the migration of the cell front was analyzed in ImageJ.

For the colony formation assay, TNBC cells were seeded at 250 cells/well for HCC1395, MDA-MB-231 and HCC38; 500/well for MBA-MB-468; 750/well for BT-20 and 1000/well for HCC1806 in 6-well plates. Next day, the medium was replaced with the one containing indicated concentrations of tested compound. Colonies of 70–100 cells were formed after 8–14 days, were fixed by incubation in 4% PFA in 1xPBS, pH 7.4 and visualized by staining with the crystal violet solution, and the number of colonies was counted.

4.3.4. Animal xenografted tumor growth

The experiments were approved by the Swiss Federal Veterinary Office and were carried out in accordance with the local animal welfare act. For experiments with BRC0016 PDX xenograft, ca. 500cm3 freshly extracted tumors from 2 donor animals were chopped into small pieces using scissors and digested using Accumax for at 1 h on a rotary shaker. After sedimentation of the large undissolved chunks, the supernatant was centrifuged at 300g for 5 min, and the resulting cell pellet was resuspended in Matrigel at the ratio of 50 μl per recipient NOD/SCID-γ (NSG) mouse (6 in total). As soon as the tumor volume reached ~100 mm^3 as measured by electronic calipers, the mice were separated into two equal groups each including N = 3 animals. The mice were injected IP daily with 20 mg/kg MU17 solution in 10% Kolliphor (Sigma) and 10% EtOH in water carrier solution. Tumor volume (mm3) was determined using the following formula: tumor volume = length × (width)2 × π/6. The drug treatment was started as soon as the tumor reached the volume of ~100mm3.

4.3.5. Slide preparation and immunofluorescent staining

After removal from the animals, tumors were photographed, sliced into fragments of ~300–400mm3 and rinsed in the excess of ice-cold 1xPBS. Subsequently, they were fixed in fresh 10% PFA solution in 1xPBS for 3–5 days at 4 °C. The tumors were embedded in paraffin blocks and cut into slices 5 μm thick in the Histology facility of University of Geneva. The slices were mounted on glass slides and stored at 4 °C. For the staining, the slides were first deparaffinized in three changes each of xylene, sequence of water mixtures of EtOH with decreasing concentrations (95%, 70% and 50%) and finally water. Subsequently, antigen retrieval was performed in 20 mM Tris-EDTA, pH 9.0 with 0.1% Tween-20 by heating up the slides to 95 °C for 20min and gradual cooling to the room temperature. Further, the slides were blocked in 1xPBS/0.1% Triton X-100 with 3% of normal horse serum and stained with primary antibodies against β-catenin (BD Biosciences), Ki67 (BD Biosciences) at 1:200 dilution. Cleaved caspase-3 staining was performed using corresponding antibodies (CST) at 1:1000 dilution and developed using SuperBoost tyramide enhancer kit (Invitrogen). The slides were mounted using the VectaSchield mounting

nuclear β-catenin and ratio between cytoplasmic and phospho- β-catenin (E) demonstrates that upon 5h treatment, **MU17** does not affect beta-catenin phosphorylation or nuclear translocation. Statistical significance was assessed by one-way ANOVA. N = 3, *p* values are reported as on Fig. 1.

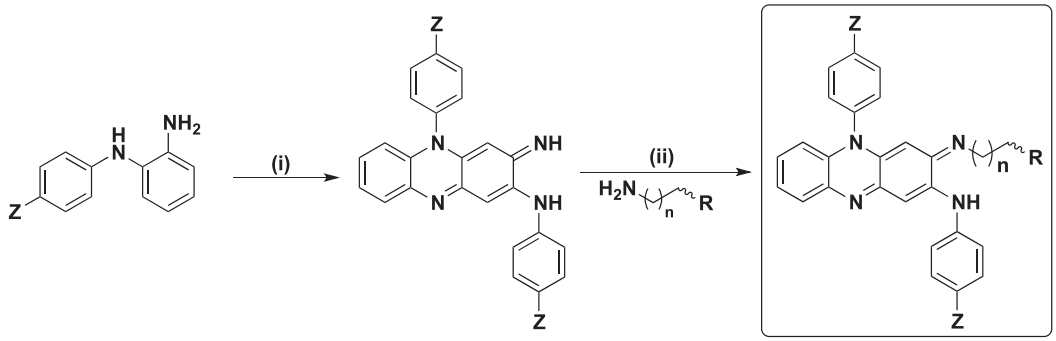

Scheme 1. Symmetrically substituted riminophenazines. Reagents and conditions: (i) $FeCl_3$, $HCl_{(aq)}$ and CH_3COOH, r.t.; (ii) Reflux in dioxane.

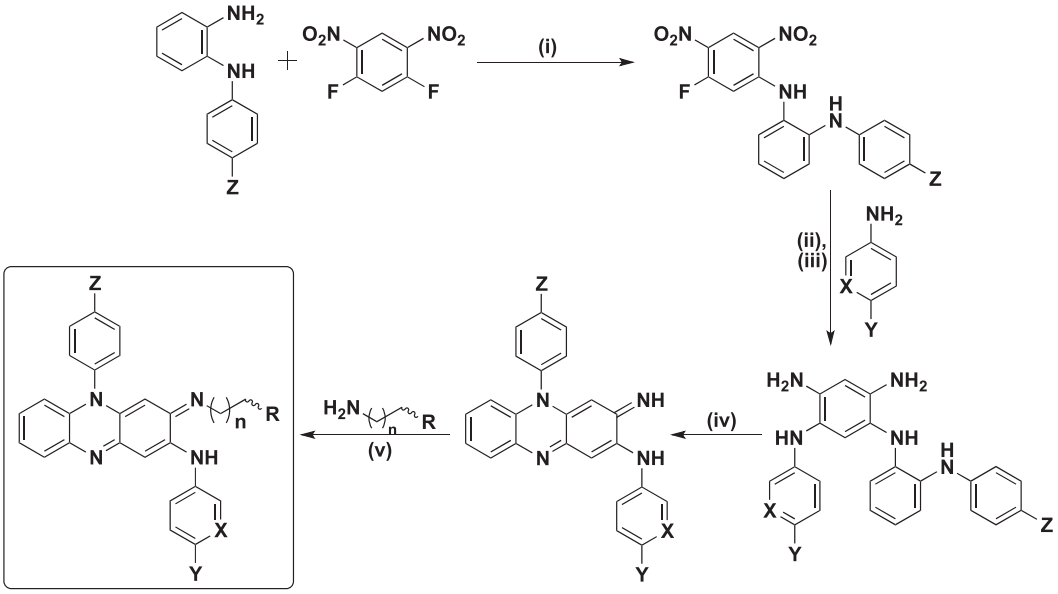

Scheme 2. Asymmetrically substituted riminophenazines. Reagents and conditions: (i) TEA, EtOH, r.t.; (ii) TEA, THF, 60 °C; (iii) AcOH, Zn(0), 0 °C → r.t.; (iv) MeOH, r.t; (v) Reflux in dioxane.

medium and visualized using AiryScan LSM-880 confocal microscope (Zeiss). For scoring, each of the stained slides was assigned with perceived level of membrane or cytoplasmic staining ranging from 0 (not observed) to 5 (maximum) and average score for all the stained tumors was calculated for presentation.

4.3.6. Immunofluorescent staining of the cultured cells

The indicated cell lines were seeded at 200 000 cells/well in the 6-well plates with poly-L-lysine-coated coverslips on the bottom. After 5h of treatment with or without Wnt3a in presence or absence of MU17, the cells were washed 2x by PBS, fixed by 4%PFA at room temperature and stained and visualized as described above for tumor samples. The antibodies used for staining were against β-catenin (BD Biosciences) and pS33/37/T41-β-catenin (CST).

4.3.7. Western blotting

TNBC cell lines were seeded at 100 000 cells/well in 24 well plates. The next day, the medium was replaced with fresh medium containing drug pre-warmed at 37 °C. After further 24h incubation, the medium was removed, followed by washing with 500 μl of 1x PBS twice per well. The cells were lysed in the well by addition of 30 μl of ice-cold RIPA buffer (1x TBS, 4 mM EDTA, 1% Triton, 0.1% SDS, 1x Protease inhibitor cocktail (Roche)) and incubated on ice for 10min. The cells were resuspended and then centrifuged at 18000g at 4 °C to remove debris. 5 μl of the supernatants each were further analyzed by Western blot with antibodies against active β-catenin (Millipore) and α-Tubulin (Sigma) at 1:1000 dilutions.

4.3.8. Evaluation of in vivo compound levels

On the last day of the trial, NOD/SCID-γ (NSG) mice bearing intramammary tumors were injected IP as described above and sacrificed 3 h afterwards. Immediately upon sacrifice the tumor and liver samples were collected and frozen on dry ice. The samples were weighted and extracted by 2 min homogenisation on a ball beater with at least 3 vol parts of ice cold CH_3CN (more in case of low amounts of material to provide enough homogenisation volume) containing an internal standard (compound **MU25** (**40**)) The samples were centrifuged at 16 000g, 10min, 4 °C and the supernatant was diluted with H_2O to a final concentration of 25% CH_3CN. After repetition of the centrifugation, the samples were quantified by LC-MS on the Q Exactive instrument (ThermoFisher) in positive mode with electrospray ionization. Briefly, 10 μl of sample were injected into the reverse-phase HPLC column (Zorbax Eclipse Plus C18, Agilent Technologies) and separated using a gradient from 25

to 95% CH_3CN with 0.1% formic acid. The peaks corresponding to the compounds ([M+H]+) were identified and quantified using the Xcalibur software and with the help of a standard curve (0.3 μM−100 μM, 6 concentrations) built from known compound dilutions in control blood plasma and extracted in the same batch with the samples.

4.4. Evaluation of compounds solubility

As all the compounds have strong absorbance in the visible part of spectrum, their solubility was assessed by spectrophotometry. Compounds (2−3 mg) were dissolved in PBS buffer pH 7.4 at a concentration of 200 mg/ml (**GG08**, **GG13**, **MU05**, **MU17**, **MU23)** or at a concentration of 50 mg/ml (**AR13** and **AR18**). After 3 h of shaking they were centrifuged at 20000g for 30 min. Supernatant (1 μl) was taken and diluted 4000x folds to create sample. For all other less soluble compounds (see Supporting Table S1), the compound was added from DMSO stock to create a target concentration of 250 μg/ml (final concentration of DMSO was 0.5% in all cases). After 3h of incubation on shaker, the solution was centrifuged at 20000g for 30 min. The supernatant was used to quantify the compound solubility.

For quantification of the concentration of the compound in the supernatants, the calibration curves of the compounds ranging from 1.5 to 50 μg/ml were made on Tecan Infinite M200 plate reader. For maximal sensitivity, the peak absorbance of the compound was measured and the corresponding maximum wavelength was used (490 nm for **GG08**, **MU05**, **MU17**, **MU23**, **AR13** and **AR18**; 470 nm for **GG13**; 450 nm for clofazimine and 460 nm for all others). For the most soluble compounds (see above) the calibration curves were made directly in PBS, for all the least soluble compounds the calibration curves were made in 50% DMSO in PBS and for clofazimine and **GM05** − in 75% DMSO in PBS. The supernatant samples were supplied with corresponding amount of DMSO prior to mesurement. The data was fit and interpolated in Prism 7.0 (GraphPad).

Author information

Corresponding authors: E-mail: vladimir.katanaev@unige.ch, anna.sparatore@unimi.it, Phones: (+41) 22 379 5353, (+39) 02 503 19 365.

Funding

This work was supported by the Novartis Foundation for Medical-Biological Research, grant #17C153 to V.L.K.; J.X. was recipient of the Theodor et Gabriela Kummer PhD fellowship (University of Lausanne)

Declaration of competing interest

The authors declare that they have no known competing financial interests or personal relationships that could have appeared to influence the work reported in this paper.

Abbreviations

TNBC	triple-negative breast cancer
MTT	3-(4,5-dimethylthiazol-2-yl)-2,5-diphenyltetrazolium bromide (thiazolyl blue)
HRMS	high-resolution mass spectrometry
DCM	dichloromethane
PDX	patient-derived xenograft

Appendix A. Supplementary data

Supplementary data to this article can be found online at https://doi.org/10.1016/j.ejmech.2021.113562.

References

[1] S. Pushpakom, F. Iorio, P.A. Eyers, K.J. Escott, S. Hopper, A. Wells, A. Doig, T. Guilliams, J. Latimer, C. McNamee, A. Norris, P. Sanseau, D. Cavalla, M. Pirmohamed, Drug repurposing: progress, challenges and recommendations, Nat. Rev. Drug Discov. 18 (2019) 41−58, https://doi.org/10.1038/nrd.2018.168.
[2] A. Astolfi, T. Felicetti, N. Iraci, G. Manfroni, S. Massari, D. Pietrella, O. Tabarrini, G.W. Kaatz, M.L. Barreca, S. Sabatini, V. Cecchetti, Pharmacophore-based repositioning of approved drugs as novel Staphylococcus aureus NorA efflux pump inhibitors, J. Med. Chem. 60 (2017) 1598−1604, https://doi.org/10.1021/acs.jmedchem.6b01439.
[3] N. Novac, Challenges and opportunities of drug repositioning, Trends Pharmacol. Sci. 34 (2013) 267−272, https://doi.org/10.1016/j.tips.2013.03.004.
[4] V.L. Katanaev, The Wnt/Frizzled GPCR signaling pathway, Biochem. Biokhimiia. 75 (2010) 1428−1434.
[5] Z. Steinhart, S. Angers, Wnt signaling in development and tissue homeostasis, Dev. Camb. Engl. 145 (2018), https://doi.org/10.1242/dev.146589.
[6] A. Koval, V.L. Katanaev, Dramatic dysbalancing of the Wnt pathway in breast cancers, Sci. Rep. 8 (2018) 7329, https://doi.org/10.1038/s41598-018-25672-6.
[7] L.R. Howe, A.M.C. Brown, Wnt signaling and breast cancer, Canc. Biol. Ther. 3 (2004) 36−41, https://doi.org/10.4161/cbt.3.1.561.
[8] A. Blagodatski, D. Poteryaev, V.L. Katanaev, Targeting the Wnt pathways for therapies, Mol. Cell. Ther. 2 (2014) 28, https://doi.org/10.1186/2052-8426-2-28.
[9] H.V. Shaw, A. Koval, V.L. Katanaev, Targeting the Wnt signalling pathway in cancer: prospects and perils, Swiss Med. Wkly. 149 (2019) w20129, https://doi.org/10.4414/smw.2019.20129.
[10] K. Ahmed, A. Koval, J. Xu, A. Bodmer, V.L. Katanaev, Towards the first targeted therapy for triple-negative breast cancer: repositioning of clofazimine as a chemotherapy-compatible selective Wnt pathway inhibitor, Canc. Lett. 449 (2019) 45−55, https://doi.org/10.1016/j.canlet.2019.02.018.
[11] A.V. Koval, P. Vlasov, P. Shichkova, S. Khunderyakova, Y. Markov, J. Panchenko, A. Volodina, F.A. Kondrashov, V.L. Katanaev, Anti-leprosy drug clofazimine inhibits growth of triple-negative breast cancer cells via inhibition of canonical Wnt signaling, Biochem. Pharmacol. 87 (2014) 571−578, https://doi.org/10.1016/j.bcp.2013.12.007.
[12] M. Philip, J.F. Samson, P.S. Simi, Clofazimine-induced hair pigmentation, Int. J. Trichol. 4 (2012) 174−175, https://doi.org/10.4103/0974-7753.100088.
[13] Jiabin Xu, Alexey Koval, Vladimir Katanaev L, et al., Beyond TNBC: repositioning of clofazimine against a broad range of Wnt-dependent cancers, Front. Oncol. 10 (2020) 2825, https://doi.org/10.3389/fonc.2020.602817. In this issue.
[14] L. Cui, S. Mharakurwa, D. Ndiaye, P.K. Rathod, P.J. Rosenthal, Antimalarial drug resistance: literature review and activities and findings of the ICEMR network, Am. J. Trop. Med. Hyg. 93 (2015) 57−68, https://doi.org/10.4269/ajtmh.15-0007.
[15] S.G. Franzblau, K.E. White, J.F. O'Sullivan, Structure-activity relationships of tetramethylpiperidine-substituted phenazines against Mycobacterium leprae in vitro, Antimicrob. Agents Chemother. 33 (1989) 2004−2005, https://doi.org/10.1128/aac.33.11.2004.
[16] A. Barteselli, M. Casagrande, N. Basilico, S. Parapini, C.M. Rusconi, M. Tonelli, V. Boido, D. Taramelli, F. Sparatore, A. Sparatore, Clofazimine analogs with antileishmanial and antiplasmodial activity, Bioorg. Med. Chem. 23 (2015) 55−65, https://doi.org/10.1016/j.bmc.2014.11.028.
[17] I. Bassanini, S. Parapini, N. Basilico, A. Sparatore, Novel hydrophilic riminophenazines as potent antiprotozoal agents, ChemMedChem 14 (2019) 1940−1949, https://doi.org/10.1002/cmdc.201900522.
[18] M. Tonelli, F. Novelli, B. Tasso, A. Sparatore, V. Boido, F. Sparatore, S. Cannas, P. Molicotti, S. Zanetti, S. Parapini, R. Loddo, Antitubercular activity of quinolizidinyl/pyrrolizidinylalkyliminophenazines, Bioorg. Med. Chem. 22 (2014) 6837−6845, https://doi.org/10.1016/j.bmc.2014.10.035.
[19] T.J. Cheeseright, M.D. Mackey, J.L. Melville, J.G. Vinter, FieldScreen: virtual screening using molecular fields. Application to the DUD data set, J. Chem. Inf. Model. 48 (2008) 2108−2117, https://doi.org/10.1021/ci800110p.
[20] A. Jahn, G. Hinselmann, N. Fechner, A. Zell, Optimal assignment methods for ligand-based virtual screening, J. Cheminf. 1 (2009) 14, https://doi.org/10.1186/1758-2946-1-14.
[21] I. Bassanini, S. Parapini, C. Galli, N. Vaiana, A. Pancotti, N. Basilico, D. Taramelli, S. Romeo, Discovery and pharmacophore mapping of a low-nanomolar inhibitor of P. Falciparum growth, ChemMedChem 14 (2019) 1982−1994, https://doi.org/10.1002/cmdc.201900526.
[22] J. Karlsson, A. Ungell, J. Gråsjö, P. Artursson, Paracellular drug transport across intestinal epithelia: influence of charge and induced water flux, Eur. J. Pharm. Sci. Off. J. Eur. Fed. Pharm. Sci. 9 (1999) 47−56, https://doi.org/10.1016/s0928-0987(99)00041-x.
[23] E. López-Knowles, S.J. Zardawi, C.M. McNeil, E.K.A. Millar, P. Crea, E.A. Musgrove, R.L. Sutherland, S.A. O'Toole, Cytoplasmic localization of beta-

catenin is a marker of poor outcome in breast cancer patients, Cancer Epidemiol. Biomark. Prev. Publ. Am. Assoc. Cancer Res. Cosponsored Am. Soc. Prev. Oncol. 19 (2010) 301–309, https://doi.org/10.1158/1055-9965.EPI-09-0741.

[24] M.S. Rao, R. Gupta, M.J. Liguori, M. Hu, X. Huang, S.R. Mantena, S.W. Mittelstadt, E.A.G. Blomme, T.R. Van Vleet, Novel computational approach to predict off-target interactions for small molecules, Front. Big Data. 2 (2019), https://doi.org/10.3389/fdata.2019.00025.

[25] H.-H. Lin, L.-L. Zhang, R. Yan, J.-J. Lu, Y. Hu, Network analysis of drug-target interactions: a study on FDA-approved new molecular entities between 2000 to 2015, Sci. Rep. 7 (2017) 12230, https://doi.org/10.1038/s41598-017-12061-8.

[26] T. Cheng, M. Hao, T. Takeda, S.H. Bryant, Y. Wang, Large-scale prediction of drug-target interaction: a data-centric review, AAPS J. 19 (2017) 1264–1275, https://doi.org/10.1208/s12248-017-0092-6.

[27] K. Ahmed, H.V. Shaw, A. Koval, V.L. Katanaev, A second WNT for old drugs: drug repositioning against WNT-dependent cancers, Cancers 8 (2016), https://doi.org/10.3390/cancers8070066.

[28] V.C. Barry, J.G. Belton, M.L. Conalty, J.M. Denneny, D.W. Edward, J.F. O'sullivan, D. Twomey, F. Winder, A new series of phenazines (Rimino-Compounds) with high antituberculosis activity, Nature 179 (1957) 1013–1015, https://doi.org/10.1038/1791013a0.

[29] J. Xu, B. Wang, L. Fu, H. Zhu, S. Guo, H. Huang, D. Yin, Y. Zhang, Y. Lu, In vitro and in vivo activities of the riminophenazine TBI-166 against Mycobacterium tuberculosis, antimicrob, Agents Chemother 63 (2019), https://doi.org/10.1128/AAC.02155-18.

[30] M.C. Cholo, H.C. Steel, P.B. Fourie, W.A. Germishuizen, R. Anderson, Clofazimine: current status and future prospects, J. Antimicrob. Chemother. (2011) dkr444, https://doi.org/10.1093/jac/dkr444.

[31] P. Gurfinkel, J.C. Pina, M. Ramos-e-Silva, Use of clofazimine in dermatology, J. Drugs Dermatol. JDD 8 (2009) 846–851.

[32] H. Tazarki, W. Zeinyeh, Y.J. Esvan, S. Knapp, D. Chatterjee, M. Schröder, A.C. Joerger, J. Khiari, B. Josselin, B. Baratte, S. Bach, S. Ruchaud, F. Anizon, F. Giraud, P. Moreau, New pyrido[3,4-g]quinazoline derivatives as CLK1 and DYRK1A inhibitors: synthesis, biological evaluation and binding mode analysis, Eur. J. Med. Chem. 166 (2019) 304–317, https://doi.org/10.1016/j.ejmech.2019.01.052.

[33] D. Zhang, Y. Lu, K. Liu, B. Liu, J. Wang, G. Zhang, H. Zhang, Y. Liu, B. Wang, M. Zheng, L. Fu, Y. Hou, N. Gong, Y. Lv, C. Li, C.B. Cooper, A.M. Upton, D. Yin, Z. Ma, H. Huang, Identification of less lipophilic riminophenazine derivatives for the treatment of drug-resistant tuberculosis, J. Med. Chem. 55 (2012) 8409–8417, https://doi.org/10.1021/jm300828h.

[34] A. Koval, V.L. Katanaev, Wnt3a stimulation elicits G-protein-coupled receptor properties of mammalian Frizzled proteins, Biochem. J. 433 (2011) 435–440, https://doi.org/10.1042/BJ20101878.